



# Plastic Deformation Mechanism of the Ti6Al4V Micro-gear Formed Under an Electrical Field

Bo Zeng<sup>1,2</sup> · Xiangzhong Yan<sup>1,2</sup> · Zhiqiang Xie<sup>3</sup> · Jian Liu<sup>1</sup> · Jie Wang<sup>1,2</sup> · Kunlan Huang<sup>1,2</sup> · Yi Yang<sup>1</sup>

Received: 12 April 2023 / Revised: 28 June 2023 / Accepted: 3 July 2023 / Published online: 17 July 2023  
© The Author(s), under exclusive licence to Korean Society for Precision Engineering 2023

## Abstract

Despite the fact that titanium alloy micro-gear has superior performance and can withstand special conditions, it is difficult to machine due to its poor plasticity and high strength. We proposed an eco-friendly, efficient, and sustainable electric field assisted micro-plastic forming technology (micro-EFAPFT) for forming titanium alloy microparts. Ti-6Al-4 V alloy bars were extruded into micro-gears using an electrothermal coupling field and Joule heating in a graphite mold. The micro-gear has high precision, good surface quality, and a simple process. The whole process takes only 380 s. The findings demonstrate that the best gear forming degree, fewer microstructure defects, and hardness reaching 330.1 HV—4.4% higher than that of the raw material—occur when the pressure holding period is 120 s. During the plastic deformation process, phase transformation and recrystallization occur, increasing the fraction of  $\alpha$  phase from 96.6–99.68% and increasing the grain orientation difference. The tooth tip has finer grains but longer dislocation lines. In conclusion, the electric field accelerates dislocation motion, reduces dislocation density, and increases material plasticity, allowing the Ti6Al4V micro-gear to be formed in a single step. The experimental results validate the feasibility of this technology for producing titanium alloy micro-gear and can be used to guide the production of different materials and shapes of microparts.

**Keywords** Titanium alloy · Micro-gear · Environmental-friendly · Electrical field · One-step forming

## 1 Introduction

Over the past decade, the trend toward compact, integrated and miniaturization of products such as micro-aerial vehicles (MAV), micro-robots, sensor and actuators has continued. This trend calls for miniaturization of components from mesoscopic to microscale [1, 2]. Micromachining technology has developed greatly, making it possible to design and develop ever smaller and more complex miniaturized products [3–6]. However, because of the slow and ordinal nature of the procedure, it is not suitable for mass production, such technique results in a high cost, and it is heavily dependent on technologies and machining tools [7–10]. Therefore, many researchers have put forward the micro-plastic forming technology, which has the advantages of high productivity, low material loss, good mechanical properties and small tolerance, as a kind of micro-manufacturing technology with great development prospects [11–14].

To explore micro components as the micro-aerial vehicles (MAV) or micro-robots, one of the critical factors is the micro-parts manufacturing. In micro aircraft, it is necessary to transfer power precisely and change the direction of motion, which puts forward higher requirements on the dimensional accuracy

✉ Kunlan Huang  
huangkunlan@scu.edu.cn

Bo Zeng  
zengb1995@163.com

Xiangzhong Yan  
30950809@qq.com

Zhiqiang Xie  
929364134@qq.com

Jian Liu  
liujian@scu.edu.cn

Jie Wang  
wangjie@scu.edu.cn

Yi Yang  
yangyi@scu.edu.cn

<sup>1</sup> School of Mechanical Engineering, Sichuan University, Chengdu 610065, Sichuan, People's Republic of China

<sup>2</sup> Yibin Industrial Technology Research Institute of Sichuan University, Yibin 644005, Sichuan, People's Republic of China

<sup>3</sup> AECC AERO Science and Technology Co., Ltd, Chengdu 610503, Sichuan, People's Republic of China

and mechanical properties of micro-gears [15, 16]. Titanium alloy is widely utilized in the aircraft and navigation industries, as well as medical devices, due to its good mechanical qualities, outstanding corrosion resistance, and biocompatibility [17–19]. However, the deformation resistance of titanium alloy is high and usually a serious spring-back is present at the room temperature, which brings a challenge to the precise large deformation process of cylinder or the variable curvature part of the titanium alloy [20, 21]. Nowadays, the drawbacks of the micro-plastic forming technology are associated with (i) material types (limited to copper, Aluminum and magnesium, etc. with low strength, good plasticity and low melting temperature.) [22–25] and (ii) component geometries which are limited to 2D (Micro tensile, micro compression, micro bending and micro channel, etc.) [26–28] and 2.5D (micro cup and microtubule, etc.).

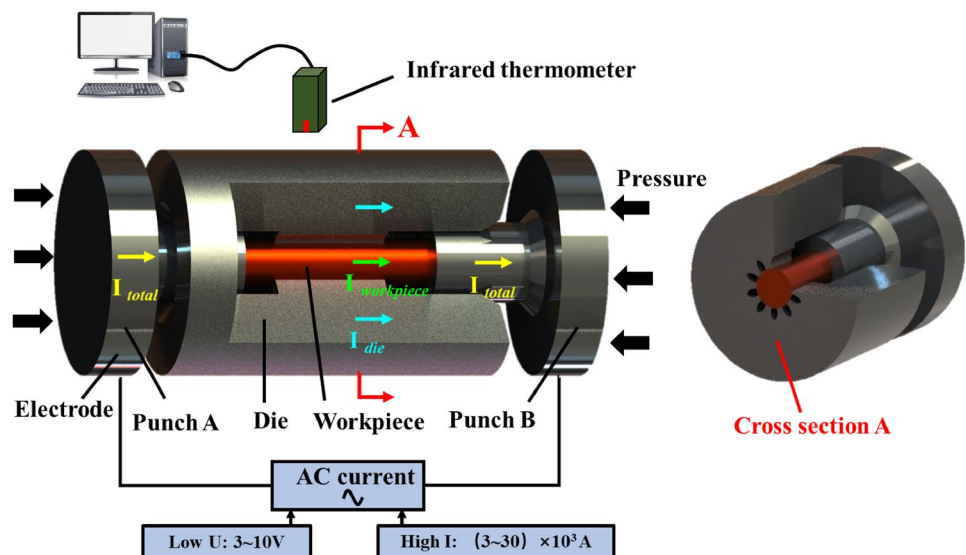
For purpose of obtaining the desired mechanical properties by controlling the microstructure, titanium alloys are usually deformed at relatively low temperatures ( $0.65\text{--}0.75 T_m$ ) [29]. However, with the decrease of deformation temperature, the thermal working property of titanium alloy decreases sharply. Therefore, the high temperature formability of titanium alloy has been studied by prior researchers. The deformation is mainly controlled by recrystallization of  $\alpha$  phase and grain boundary slip at low temperature ( $750\text{--}850^\circ\text{C}$ ) and low strain rate ( $0.001\text{--}0.1\text{s}^{-1}$ ). When the temperature is higher ( $>900^\circ\text{C}$ ) or high strain rate ( $1\text{--}10\text{s}^{-1}$ ),  $\beta$  phase dynamic recovery was the step to control the rate [30–32].

So far, many processes have been developed that use external electric field to assist the plastic forming process of Titanium alloy. Over the past decade, Taekyung Lee et al. have reported the advantages of electrically-assisted forming, including the reduction of bending force in large and miniature sheet metal [33]. After pulse electric current treatment and annealing treatment, Zhiyong Zhao discovered

that the elongation of Ti6Al4V alloy samples dramatically increased by 66.5% and 20.8%, respectively [34]. Pulse current can significantly improve the plasticity of deformed Ti6Al4V alloy, but the strength is still relatively high [35]. Existing studies have proved the feasibility of electric field assisted plastic forming of titanium alloy. Based on this, an electrical field assisted micro plastic forming technology (Micro-EFAPFT) was designed in this paper, which innovatively combined electric field assisted forming with microparts manufacturing. Ti6Al4V alloy micro-gears were prepared under the combined action of high temperature, current and forming pressure, as illustrated in Fig. 1. In the electrical field-assisted micro-forming method, the Ti6Al4V titanium alloy micro-gear was created under the coinstantaneous action of high temperature, current and forming pressure. Initially, the workpiece is placed directly into a small mold, and an AC current passes through the mold and the workpiece, generating temperature through the Joule effect to achieve heating. Pressure is applied to both ends of the sample. The micro-gear is formed in one step and the whole process takes less than 4 min. The traditional sintering method requires large heating space, long holding time and consumes a lot of energy. While Micro-EFAPFT is an environmentally friendly production mode with small heating cavity, concentration temperature and short forming time. The traditional gear production mode is forging and machining, the utilization rate of raw materials is low. This technique is a sustainable development practice for the integral gear once forming, avoid producing waste.

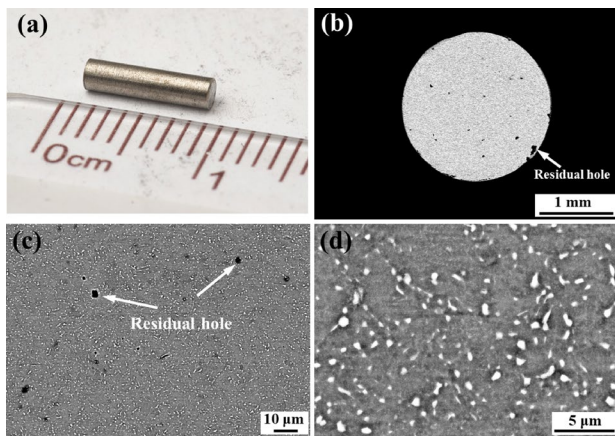
To the best of the author's knowledge, there are few reports on the plastic forming of Ti6Al4V alloy micro-gears. The aim of this study is to process Ti6Al4V micro-gear with the Micro-EFAPFT and study its plastic deformation mechanism. The electric field assisted plastic forming method presented in this study can be used to manufacture titanium alloy micro-gear, and

**Fig. 1** Forming process diagram of Ti6Al4V micro-gear under the electrical field



**Table 1** Ti6Al4V titanium alloy bar standard composition

Composition	Fe	C	N	O	Al	V	Ti
Wt.%	0.2	0.03	0.01	0.15	6	4	Remain

**Fig. 2** a a Ti6Al4V workpiece with a size of  $\Phi 2 \times 8.02$  mm and b–d SEM images of the Ti6Al4V workpiece

the current heating rate is quick, reducing manufacturing time and improving material use efficiency. It is an environmentally friendly micro-gear manufacturing technology that provides an experimental and theoretical foundation for machining more micro-parts with different shapes and materials.

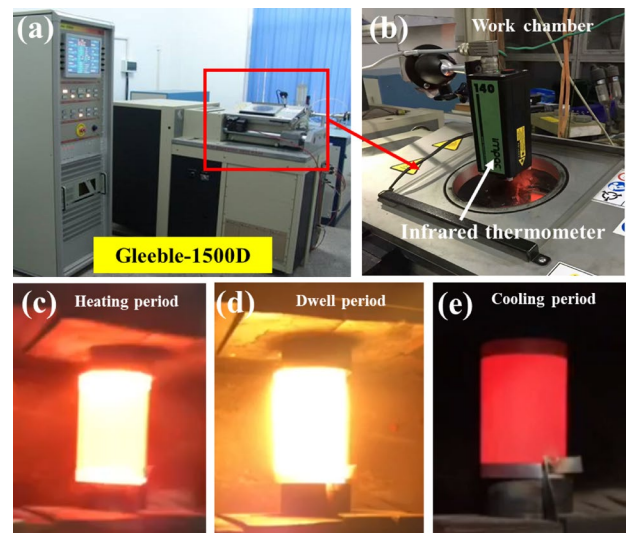
## 2 Experiment Procedures

### 2.1 Raw Materials

Ti6Al4V titanium alloy bars with a diameter of  $\Phi 2$  mm purchased from Baoji Hengchuang Metal Products Co. LTD (Shanxi, China), were used as the raw materials. Table 1 displays the chemical make-up of the Ti6Al4V titanium alloy rod. As shown in Fig. 2a, the Ti6Al4V titanium alloy bars were cut into workpieces with a size of  $\Phi 2 \times 8.02$  mm and the Fig. 2b–d show the SEM images of microstructure of the Ti6Al4V workpiece. The grains of the original Ti6Al4V rod materials exhibit a typical fine ( $\alpha + \beta$ ) equiaxed morphology and the  $\beta$  grains (light grains in Fig. 2d) are evenly distributed around the  $\alpha$  grains (dark grains in Fig. 2d). Moreover, as shown in Fig. 2b–c, the starting Ti6Al4V workpiece has a small number of residual holes.

### 2.2 Forming Process

The die-set utilized for the studies with a Gleeble-1500D thermal simulator from Dynamic System Inc., USA, is

**Fig. 3** Experimental process diagram a Gleeble-1500D, b work chamber, c–e forming process and die-set**Table 2** Technological conditions for forming micro-gear samples

Sample number	Heating rate ( $^{\circ}\text{C}/\text{s}$ )	Forming temperature ( $^{\circ}\text{C}$ )	Pressure (N)	Dwell time at the forming temperature (s)
1#	30	1200	294	5
2#	30	1200	294	60
3#	30	1200	294	120
4#	30	1200	294	180

schematically shown in Fig. 3. The machine produces a special electric field with high current and low voltage (3000~30,000 A and 3~10 V). As shown in Fig. 2a, the as-received Ti6Al4V bars are enough to form a micro involute gear with a size of modulus 0.3, tooth number 10, pitch diameter 3 mm and gear height 4 mm. A graphite die was loaded with the workpiece (Fig. 3c–e). The die containing the Ti6Al4V rod was then put into the work chamber of the Gleeble-1800D facility (Fig. 3b), where it was swiftly heated at a predetermined heating rate in a vacuum ( $< 10^{-3}$  Pa) to a certain forming temperature while applying a predetermined pressure to the punch (Fig. 3c). After then, the sample was cooled at a rate of  $20^{\circ}\text{C s}^{-1}$ . The forming process is complete when the temperature reaches room temperature (Fig. 3e). Table 2 displays the precise technological specifications of these experiments.

## 2.3 Measurements

Transmission electron microscopy (TEM) and scanning electron microscopy (JSM-5900LV, JEOL) were used to examine the samples' microstructure and backscattered electron imaging (BSE). (FEI Talos F200X) at 15kv and 200kv, respectively. Samples for TEM observation were prepared at room temperature by mechanical thinning and ion milling. A cutter with a diamond saw blade was used to cut the wafer sample from the formed sample and the final refinement of the wafer was performed using a precision ion polishing equipment (Gatan-691). A scanning electron microscope equipped with an HKL-EBSD system, the FEI Nano 430, was used to conduct an electron backscatter diffraction (EBSD) test. Vickers hardness was measured by HVS-1000 digital microhardness tester at 0.98 N load and 15s pressure holding time. Take the average of 5 measurements as the hardness of the sample.

## 3 Experimental Results and Discussion

### 3.1 The Plastic Forming Process of the Ti6Al4V gear

The sample's temperature variation and axial height reduction during the plastic forming process under an electrical field are shown in Fig. 4. As shown in Fig. 3b, an infrared thermometer (LumaSense Technologies Germany) was used to measure the forming temperature and the temperature range it can attain is 550~3300 °C. Special Limits of Error is about 0.5% when the temperature is above 1200 °C. This is a most convenient and reliable method for forming temperature monitoring in Micro-EFAPFT. The samples' actual forming temperature and preset forming temperature distribution curves show that the heating period and the first dwell time are where temperature measurement errors are most common. Due to the heat transfer, the maximum delay of the heating-up time is about 4 s. Because of the high forming temperature (1200 °C) and short measurement delay time, error range is acceptable.

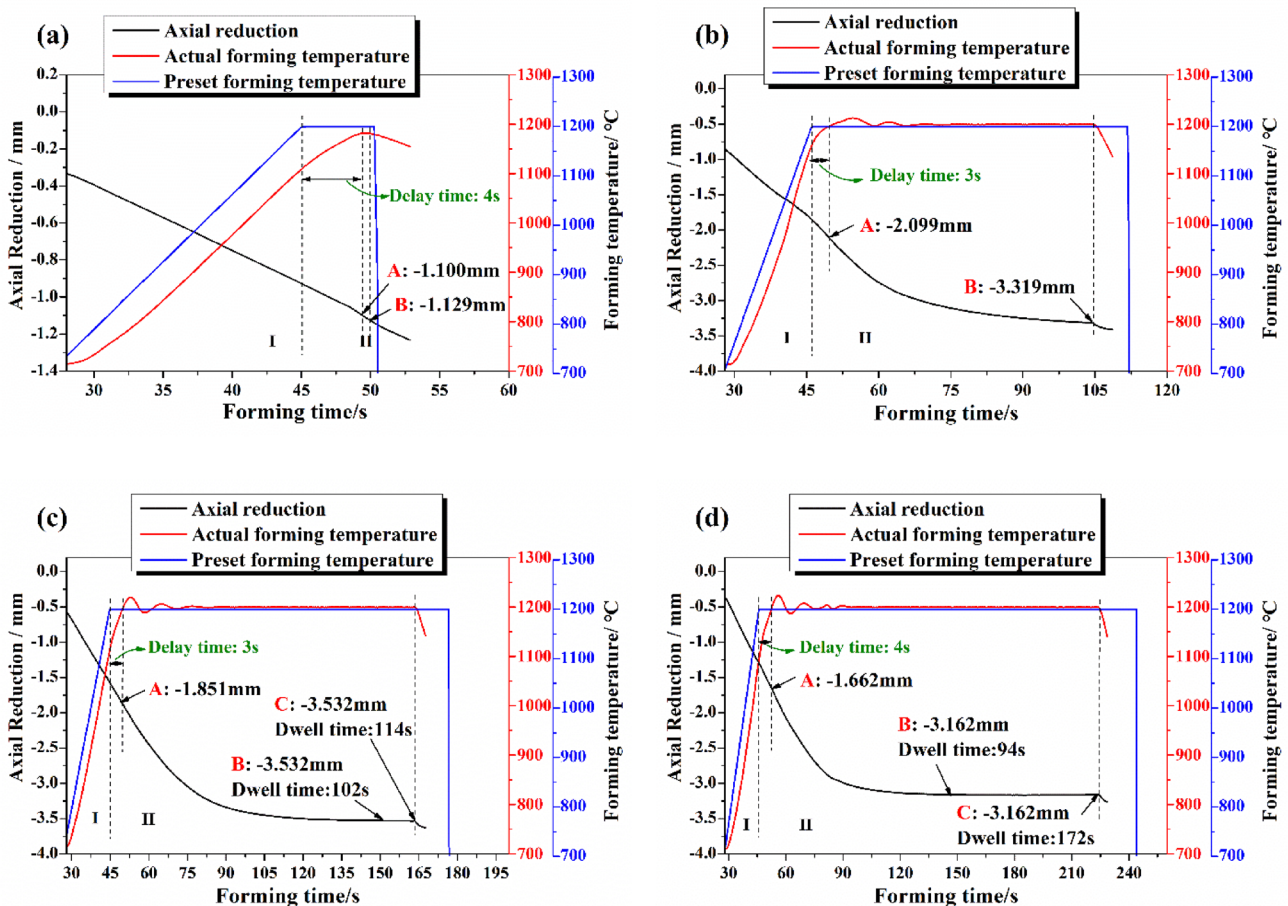


Fig. 4 The axial reduction and forming temperature of the specimens under various dwell time: a 1# 5s; b 2# 60s; c 3# 120s; d 4# 180s

By comparing the characteristics of axial reduction curve and forming temperature curve, the whole forming process includes three stages:

- i) Pre-deformation period (from the beginning to heat (20 °C) to the temperature reaches 1200 °C). As shown in Fig. 4a–d, there is a linear increase in axial reduction from the beginning of heating to point A, indicating that the original workpiece is being heated in such a short forming time.
- ii) plastic filling period (keeping at 1200 °C for a hold pressure time). As shown in Fig. 4, this period is defined as the process in which the main formability is realized. In the process of forming, the axial reduction increases rapidly and then flattens out. As shown in Fig. 4 (a-b), a more interesting thing is that there is an obviously steep axial reduction increases of the samples, and it occurs in the dwell time of less than 60s. After then, the axial reduction increases gradually. which shows that the plastic deformation process of micro-gear is not finished. Moreover, as shown in Fig. 4c–d, an axial reduction remains constant (from point B to C) after the 94~102 s dwell time. It can be found that the plastic deformation filling of the micro-gear will be finished

when the dwell time is more than 102 s. The axial reduction profiles of the warm-holding period can be used to explain the effects of the dwell time on the formability of the Ti6Al4V micro-gear.

- iii) Cooling period (time from the forming 1200 °C to room 20 °C). In Micro-EFAPFT, the rapid-cooling rate (20 °C/s) can control the material microstructure and improve the production efficiency.

### 3.2 Formability of the Ti6Al4V gear

Figure 5 shows the BSE images of the fabricated Ti6Al4V micro-gears, and the analysis results are as follows:

- i) As can be seen from the Fig. 5c, Ti6Al4V micro-gear can be well formed by plastic forming technology under the electrical field in a short time (about 2 min) with a simple forming process (one step from bar to gear). Moreover, the sample with a pressure holding time of 5s at 1200°C (Fig. 5a) has a microscopic morphology similar to that of the original workpiece (Fig. 5b–c), with residual holes. With the extension of pressure holding time, the residual pore in Ti6Al4V material significantly decreased (Fig. 5b, c). However, if the stay time is too

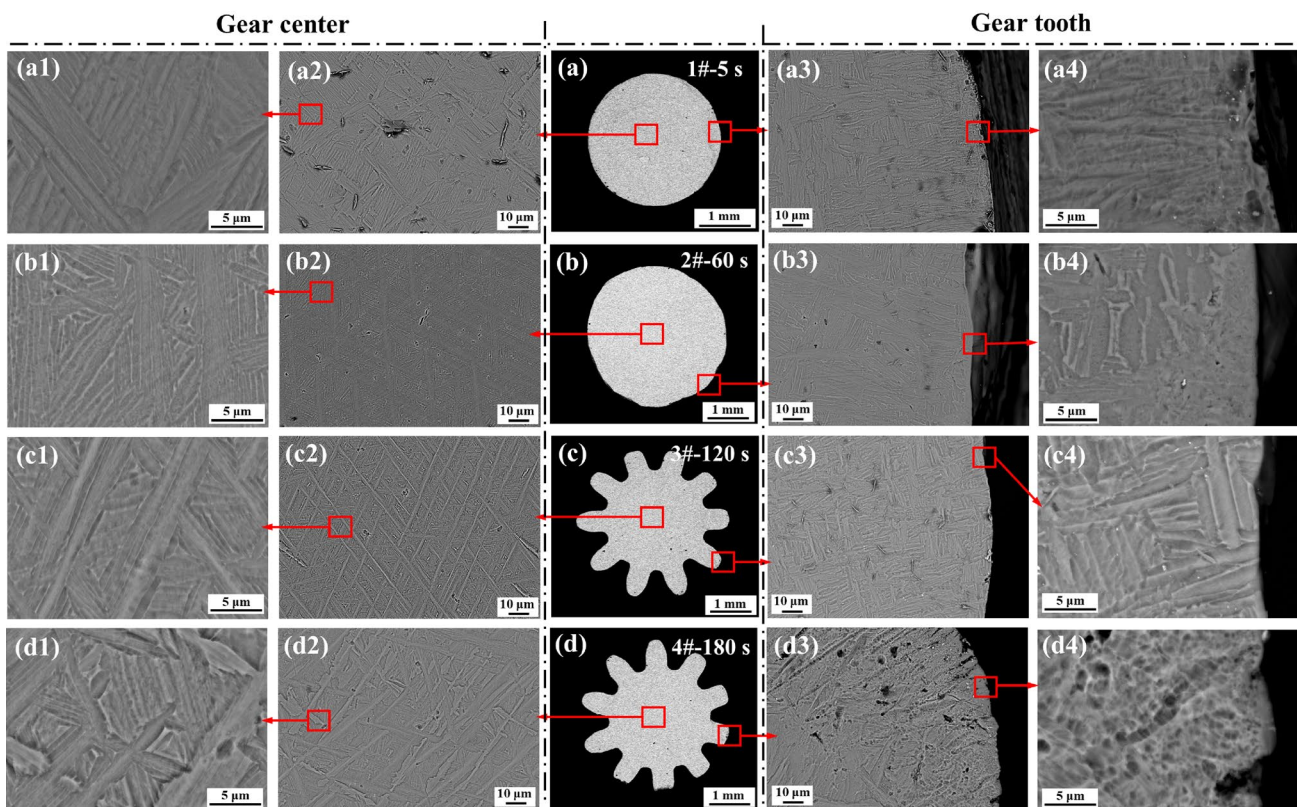


**Fig. 5** BSE micrographs of samples at different holding time: **a** 1# 5s; **b** 2# 60s; **c** 3# 120s; **d** 4# 180s; (a1-d1 and a2-d2) gear center microstructures; (a3-d3 and a4-d4) gear tooth microstructure

long (180s), a certain shrinkage cavity rate will be generated at the edge of the gear, as shown in Fig. 5 (d1–d2, d3–d4), but not at the center of the gear. The details about the surface layer model will be discussed in the following section.

- ii) Comparing the precision of size and morphology of the formed samples, the 1# (Fig. 5a) and 2# (Fig. 5b) samples are still cylindrical in shape because it lacks of sufficient time to complete the plastic deformation and plastic filling. And then, when the dwell time extends to 120 and 180 s, a good tooth shape of 3# (Fig. 5c) and 4# (Fig. 5d) samples are observed. This indicates that with the extension of forming time, the degree of plastic filling increases. The effects of dwell time on the formability on the micro-gears are corresponding with the results of the axial reduction profiles in Fig. 4.
- iii) Furthermore, comparing the microstructure of the formed samples, there is a phase transition occurred during deformation of the samples. As shown in Fig. 2, the original workpiece material has a typical fine ( $\alpha + \beta$ ) equiaxed in shape and the  $\beta$  grains can be observed obviously. However, after deformation, the material microstructure is transformed into lamellar Martensite structure, and there are long strip  $\alpha$  and  $\beta$  grains both in the center and edge of the gear. At the same time, most of the  $\beta$  phase changes to  $\alpha$  phase regardless of how long the dwell time is. It indicates that the high cooling rate results in the martensitic phase transition and the acicular  $\alpha$  will be formed [36] at the fast cooling rate ( $10^\circ\text{C/s}$ ).
- iv) A further important observation is that the difference microstructure in the gear edge and center present distinct size effect. The grains in the gear edge are shorter than those in the gear center as shown in Fig. 5 (a1, a4, b1, b4, c1, c4, d1, d4). This result is consistent with the transitional surface model, which is established to simulate the process of micro upsetting [37].

In conclusion, formability of the Ti6Al4V micro-gear was significantly influenced by the dwell time at the produced temperature.

### 3.3 Mechanical Property

Figure 6 depicts how the produced samples' Vickers hardness changed during the course of the pressure holding time at  $1200^\circ\text{C}$ . It is evident that the Vickers hardness trend and characteristics of all the produced specimens are compatible with that of formability. As can be seen from the figure, sample 3# (120s dwell time) has the highest Vickers hardness value, reaching 330.1 HV, which is 4.4% improvement over the initial material. Comparing with the original billet, all the deformed samples have a

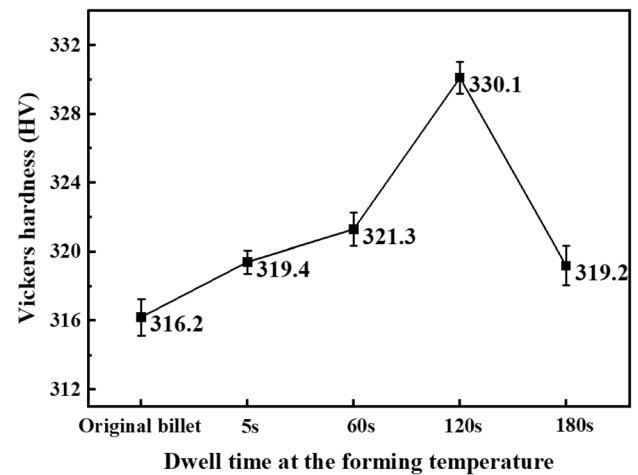


Fig. 6 Variation of Vickers hardness with Dwell time for all specimens investigated

higher hardness because the Martensite structure with the amount of more  $\alpha$  phase exhibits a higher strength after phase transformation.

### 3.4 Microstructure Evolution

#### 3.4.1 Evolution of Grain Morphology During Deformation

The evolution of the material's microstructure, including the morphology of the grains and the mobility of dislocations, is related to the formability and mechanical characteristics of micro-gear specimens [38]. In order to further understand these relationships, the microstructures of the as-received raw billet and the formed micro-gear samples were studied by EBSD analysis. The results are shown in Figs. 7 and 8. As shown in Figs. 7a and 8a, the as-received Ti6Al4V original billet contains inhomogeneous equiaxed grains with 96.64%  $\alpha$  phase and 3.36%  $\beta$  phase. The Fig. 7b–e shows the formed specimens with Widmanstatten structures and grain size of  $\alpha$  phase gradually increases with the increasing holding time. Furthermore, comparing the Fig. 8b–e with Fig. 8a, the  $\beta$  phase content of the original billet decreased significantly during plastic deformation, only about 0.32%.

The grain coarsening observed in plastic forming process is thought to be the excessive holding time [39, 40]. In our experiments, as shown in Fig. 6, grain coarsening reduces the hardness of the formed specimen when the holding time is greater than 120s. Moreover, it can be found in Fig. 5 that a short dwell time (less than 120s) will in turn reduce the dimensional accuracy of the plastic deformation of the specimen.

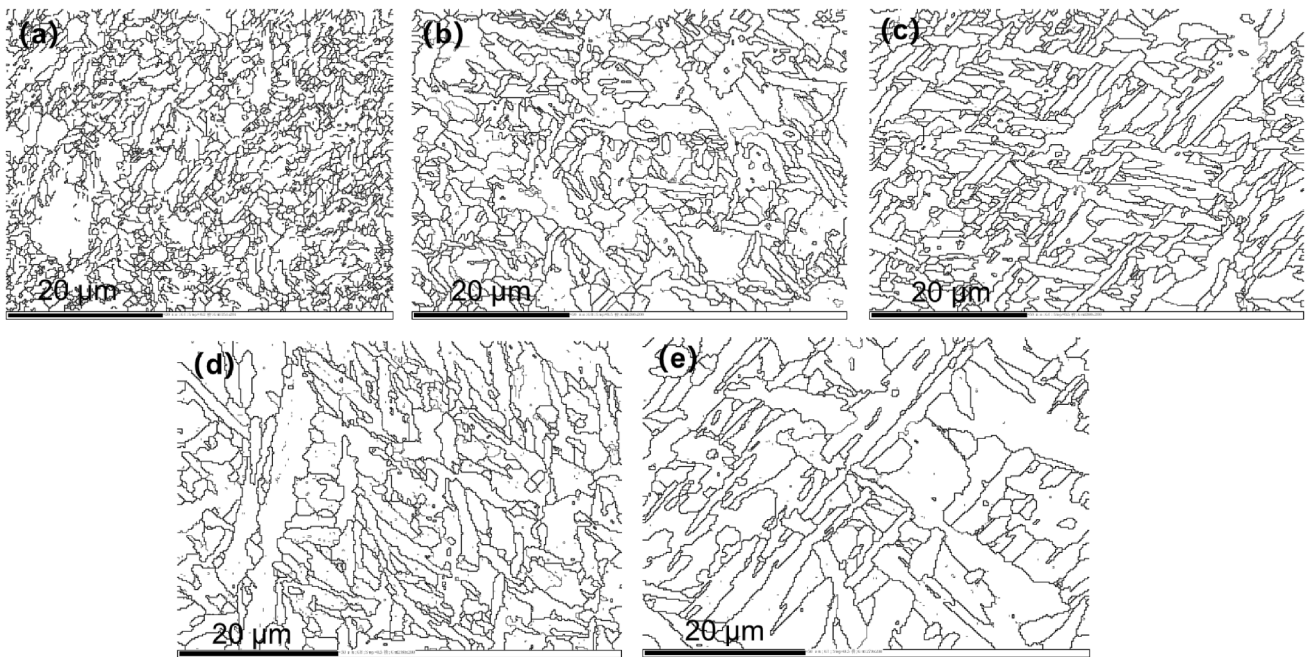


**Fig. 7** Microstructure evolution in specimens center under different plastic dwell time: **a** the original billet; **b** 1# 5s; **c** 2# 60s; **d** 3# 120s; **e** 4# 180s

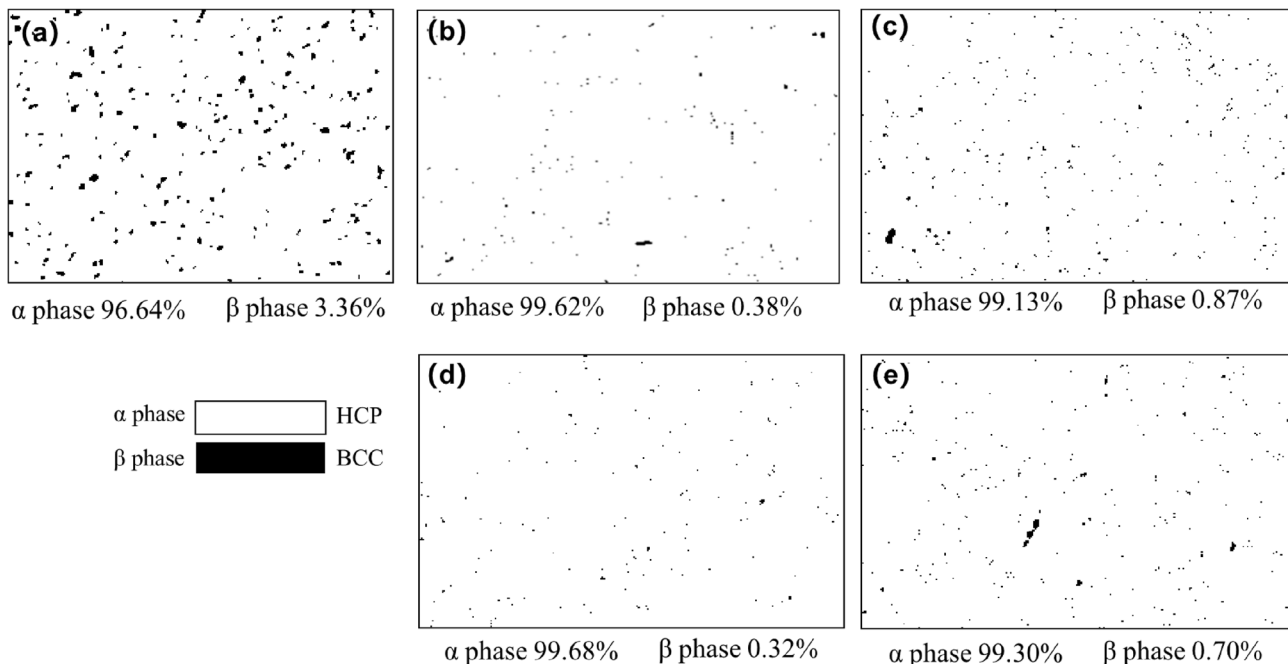


**Fig. 8** Phase composition evolution in specimens under different plastic dwell time: **a** the original billet; **b** 1# 5s; **c** 2# 60s; **d** 3# 120s; **e** 4# 180s

### 3.4.2 Recrystallization Characteristics During Deformation

As shown in Fig. 5c2 and Fig. 5c3, the microstructure of the center and tooth of the micro-gear differs considerably,

which has a crucial influence on the dimensional accuracy of the formed gear. For purpose of study the formability of the Ti6Al4V micro-gear under the electrical field, the texture and microstructure of the as-received billet, the formed gear

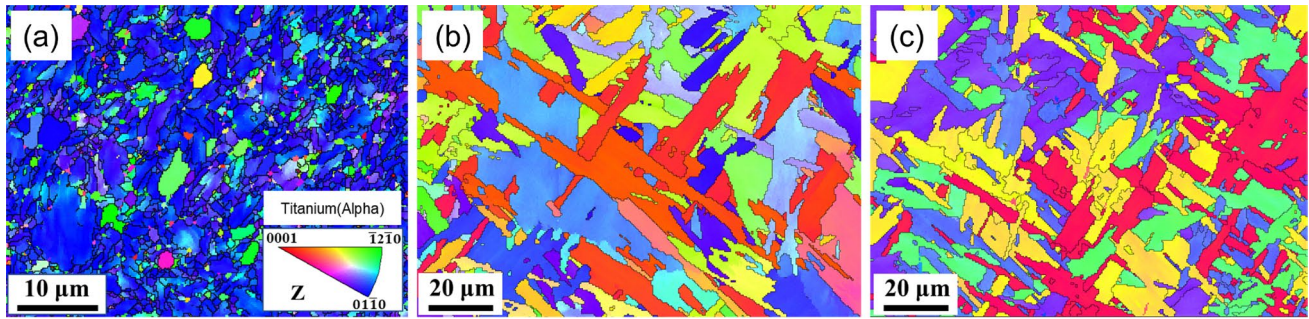


**Fig. 9** Inverse pole figure maps of  $\alpha$  laths: **a** the original billet; **b** the gear center of the 3# micro-gear; **c** the gear tooth of the 3# micro-gear

center and the gear tooth got by EBSD testing are shown in Fig. 9. It can be clearly noticed that the vital changes occurs in the texture of the specimen before and after deformation. The grain size at the tip of the gear is finer than that at the center of the gear because of the greater deformation at the tip of the gear. From Fig. 9a, the texture peaks can be noticed around  $\langle 01\bar{1}0 \rangle$ . After the deformation, as shown in Fig. 9b and c, the texture peaks are concentrated around  $\langle 0001 \rangle$  and  $\langle \bar{1}2\bar{1}0 \rangle$ . The experimental results show that the specimen undergoes phase transformation and recrystallisation during plastic deformation [41].

Furthermore, from the Fig. 10a, the Ti6Al4V material of the original billet is equiaxed crystalline within the grain, and the grain boundary orientation difference between adjacent crystals is mostly between  $2^\circ$  and  $15^\circ$ . After the deformation, as shown in Fig. 10b and c, the recrystallisation process increases the orientation difference between adjacent grains and small angular crystals within the grain become large angular grain boundaries ( $> 15^\circ$ ) [42]. The fraction of

large angular grain boundaries is greatest at the tooth tip (in Fig. 10c), so most grains are deformed grains [43].

### 3.5 Phase Transformation Characteristics

The phase characteristics is quite important because it is closely related to the mechanical property of the formed micro gear. TEM images of the phase characteristics of the specimens are shown in Fig. 11, the same experimental results as SEM (Figs. 2 and 5) and EBSD (Fig. 9), the as-received Ti6Al4V original billet contains inhomogeneous equiaxed grains with  $\alpha$  phase and  $\beta$  phase. However, the formed specimens show typical Widmanstatten structures and the phase composition is almost  $\alpha$  phase. Furthermore, as shown in Fig. 12, it can be easily found that the long strips of nanocrystals (grain 2 in Fig. 12a and grain 3 in Fig. 12f) are the  $\beta$ -phase, which exists like a sandwich structure between the  $\alpha$ -phases. The large amount of  $\alpha$  phase

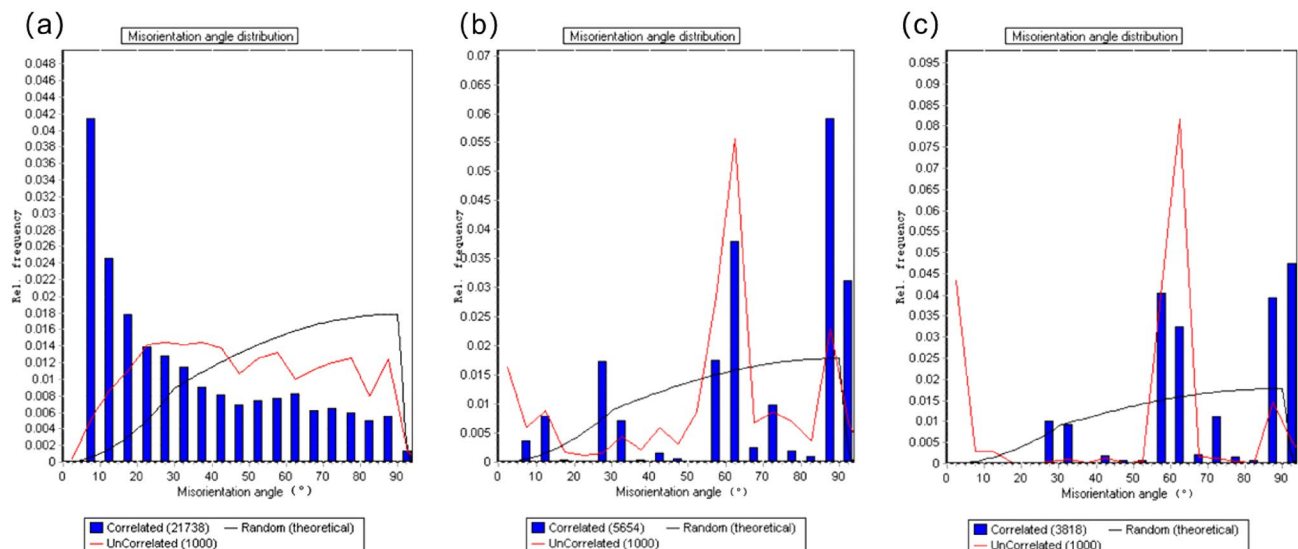


**Fig. 10** Misorientation angle distributions of the formed Ti6Al4V micro-gear in difference regions: **a** the original billet; **b** the gear center of the 3# micro-gear; **c** the gear tooth of the 3# micro-gear



**Fig. 11** TEM images of the phase characteristics of the specimens investigated: **a–c** the raw Ti6Al4V billet; **d–f** Gear center of the 3# formed sample; **g–i** Gear tip of the 3# formed sample

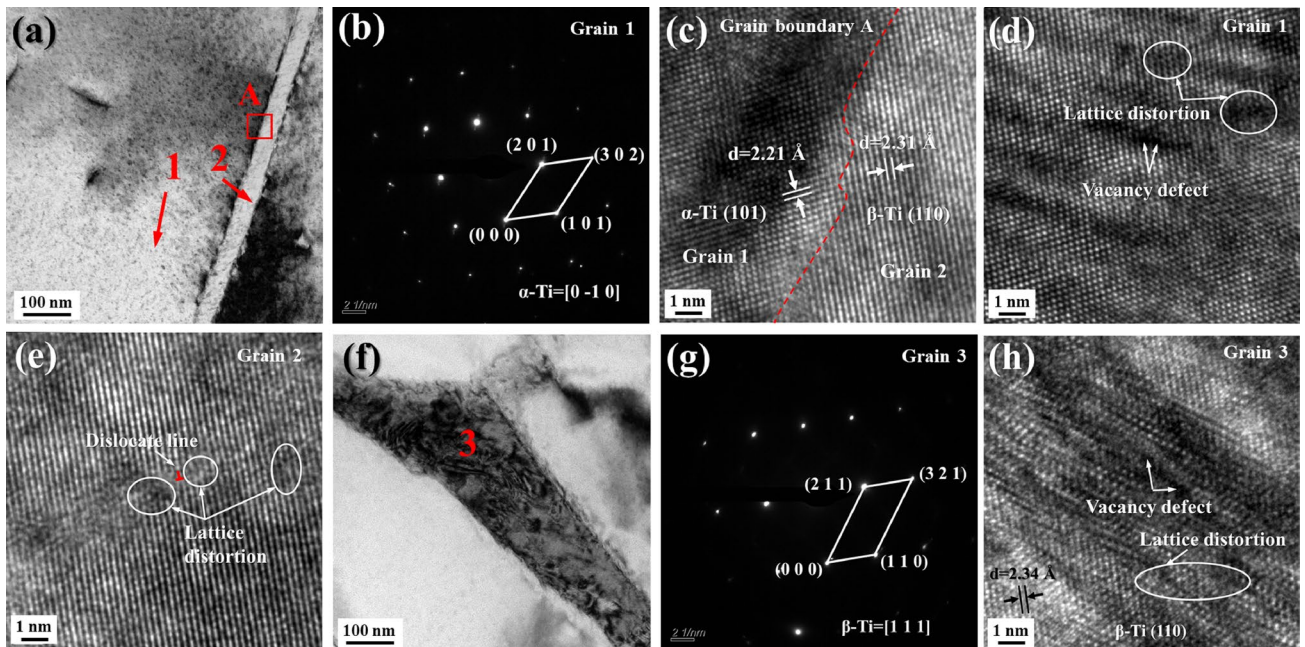
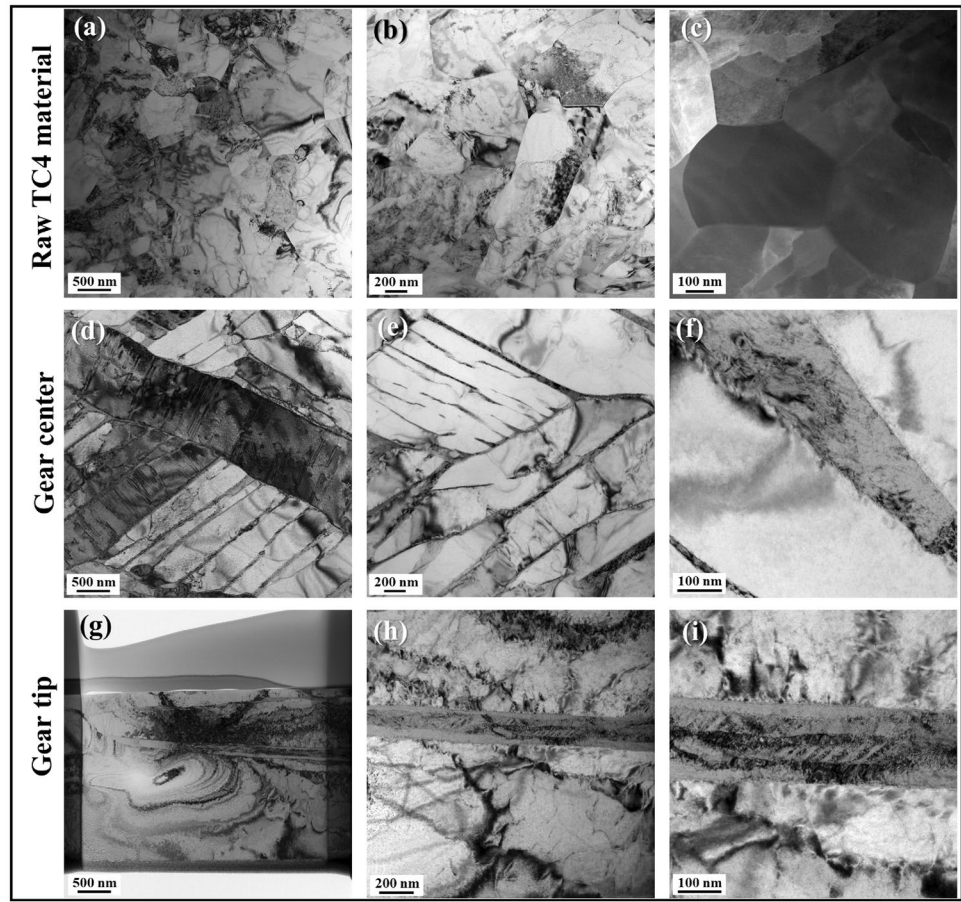


**Fig. 12** **a** and **f** TEM images of the 3# formed sample; **b** and **g** the diffraction patterns of the grain 1 and 3; **c** HRTEM image of the grain boundary A in **a**, **d**, **e** and **h** HRTEM images of the grain 1, 2 and 3 in **a**

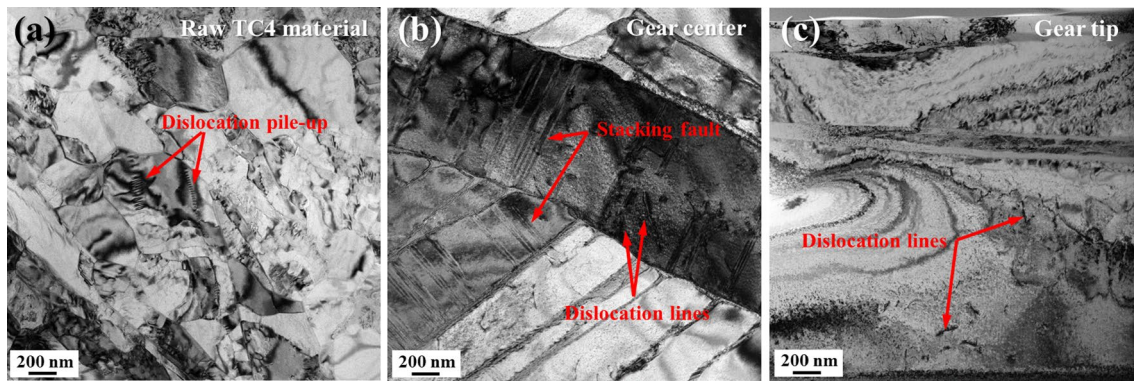


**Fig. 13** TEM images of the dislocation evolution of the specimens: **a** the raw Ti6Al4V workpiece material; **b** Gear center of the 3# formed sample; **c** Gear tip of the 3# formed sample

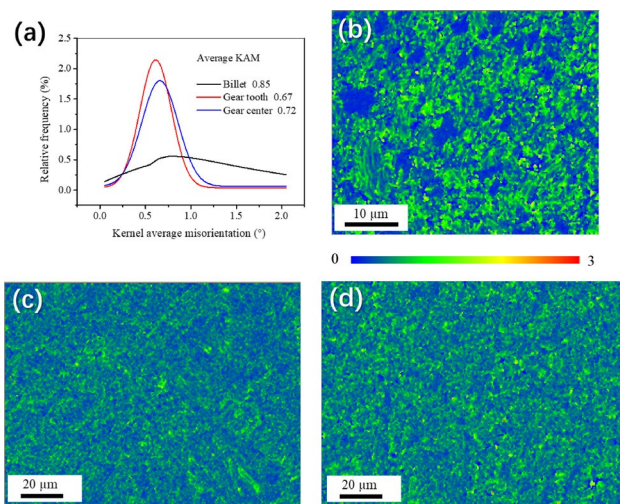


**Fig. 14** KAM maps of the specimens investigated: **a** the raw Ti6Al4V workpiece material; **b** Gear center of the 3# formed sample; **c** Gear tip of the 3# formed sample

obtained after deformation of the specimen will substantially increase the hardness of the gear [44].

### 3.6 The Effect of Electrical Field on the Dislocation Evolution

The observation of the dislocation evolution of the raw Ti6Al4V workpiece material and the deformed micro-gear through the TEM are given in Fig. 13. It can be found that there is a low dislocation density and dislocation piles up in the raw Ti6Al4V workpiece material. However, after the large deformation under the electrical field, many stacking faults and long dislocation lines (Fig. 13b) are found within the micro-gear center region. More interesting is that the micro-gear tip region has a lower dislocation density but the dislocation line is longer (Fig. 13c) than that in raw Ti6Al4V workpiece material. Moreover, Kernel Average

Misorientation (KAM) maps for the same specimens are shown in Fig. 14. Higher values of KAM indicate greater plastic deformation and a higher density of defects [45]. As can be seen in Fig. 14a, the gear tip has the largest peak value of the relative frequency of the average KAM, whereas the billet has the smallest peak value. Because of the electro-plastic effect, both the TEM and the EBSD test results demonstrate strong plastic deformation of the tooth tip under the coupling of electrothermal forces for a short period of time.

The deformation resistance is drastically decreased and the plasticity is dramatically boosted when AC or DC current is introduced to the samples while they are being deformed. This effect of the current pulses on plastic deformation of metal materials is called the electro-plastic effect [46]. In 1963, Troitskii and Lichtman first reported the interaction of moving electrons with intermediate dislocations in metal crystals [47]. According to Troitskii, the significant decrease in flow stress that occurs when metals like Zn, Cd, Sn, and Pb are subjected to a  $10^3$  A/mm<sup>2</sup> current pulse lasting 100  $\mu$ s while undergoing uniaxial tensile deformation at a constant strain rate is caused by the interaction of electrons with the elastic field of dislocations.

Nowadays, researchers [48] reported that the electro-plastic effect includes the Joule effect, pinch effect, skin effect and pure electro-plastic effect which are induced under the coupled effect of heat, electrical and force physical fields. However, about the plastic deformation process, the skin effect is more limited in industrial applications because industrial electrodes typically operate at low frequencies [49]. The relationship between the current on a conductor and the magnetic field it generates is also connected to the current on a conductor (the pinch effect). The situation that arises in the plastic deformation tests under the current circumstances, however, cannot be adequately captured by the limit of the equilibrium pinch effect that is often utilized today. The Coulombic force ( $F_c$ ) directed toward the negative electrode and the electron wind force ( $F_w$ ) exerted on the metal ions by collision with electrons floating

toward the positive electrode are the two forces that are acting on the metal atoms in this situation. The net force ( $F_{net}$ ) on an ion is:

$$F_{net} = F_w + F_c = (Z_w + Z_c)|e|E = Z^*|e|E \quad (1)$$

Where  $Z_w$  describes an ion’s capacity to pick up speed from an electron wind. (it is the charge that ion would need to have in order to produce a force that is equivalent to  $F_w$  in an electric field  $E$ :  $Z_w|e| = F_w/E$ ) and  $Z^*$  is the effective electrostatic charge ( $Z^* = Z_w + Z_c$ ).  $Z_c$  is a representation of the ion’s electrostatic charge,  $e$  is the electron charge,  $Z_w$  is dependent on the cross-section of the collisions between electrons and ions ( $\Gamma_e$ ), the main free path ( $\xi_e$ ) and the electron density ( $n_e$ ):

$$Z_w = \Gamma_e \xi_e n_e \quad (2)$$

Typically,  $Z^* \gg 0$  (being  $Z_w \gg Z_c$ ), thus, when current is driven through a metal conductor, there is a net mass flux toward the positive electrode (anode).

Moreover, other researchers also agree with that the electron wind force play a major part in the dislocation migration during the metal deformation process under the electric field [50]. Klimovt et al. give a theoretical consideration of the force of drifting electrons on dislocation in which the theoretical formula (3) is the closest to the reality [51].

$$f/l = \frac{1}{3} nm^* b v_F (v_e - v_d) = \frac{m^* b v_F J}{3e} \quad (3)$$

Where  $f/l$  denotes the force acting on the dislocation per unit length,  $n$  denotes the electron density,  $m^*$  indicates the effective electron mass,  $b$  is the Burgers vector,  $v_F$  is the Fermi velocity,  $v_e = \frac{J}{en}$  is the electron velocity, and  $v_d$  is the

dislocation velocity.  $J$  is the current density, while  $e$  is the electron charge.

Furthermore, the drift electron velocity  $v_e$  is proportional to the current density, that is, the electron wind force  $f/l$  is proportional to the current density, i.e.,

$$f/l = K_{ew} J = B_{ew} J / en \quad (4)$$

Where  $K_{ew}$  is the electron force coefficient,  $B_{ew}$  is the coefficient of the Electron wind propulsion and its value is between  $10^{-7} \sim 10^{-5}$  Nm/A.

### 3.7 Rearrangement Dislocation Structure by electro-plasticity

The Fig. 13 shows that the dislocation of the specimens changed by electric field. In general, plastic deformation is strongly associated with the creation and movement of dislocation. As shown in Figs. 15, 16 and 17, the distribution and structure of the dislocation in the samples can reflect the deformation mechanism of the Ti6Al4V micro-gear under the AC electric field, which is crucial for further understanding of the effects of electro-plasticity.

In order to observe the differences on the dislocation distribution and structure, the raw Ti6Al4V workpiece material and the formed micro-gear (include the gear center and tip) were observed by TEM in Figs. 15, 16 and 17. Figure 15 shows the undeformed specimen in which the dislocation originates in the  $\alpha$ -Ti grain boundary. Several short dislocations are orderly arranged with each other (Fig. 15a-c) and the lattice is highly deformed in the  $\alpha$ -Ti (101) plane, showing a high-density dislocation source (Fig. 15f). Figure 16

**Fig. 15** Images of the dislocation evolution of the raw Ti6Al4V workpiece material specimens investigated: **a–c** the TEM images of the raw Ti6Al4V material; **d** the diffraction pattern of the grain 1; **e** a HRTEM image of the grain 1 in **a** and **f** the lattice deformation of the box area of **e**

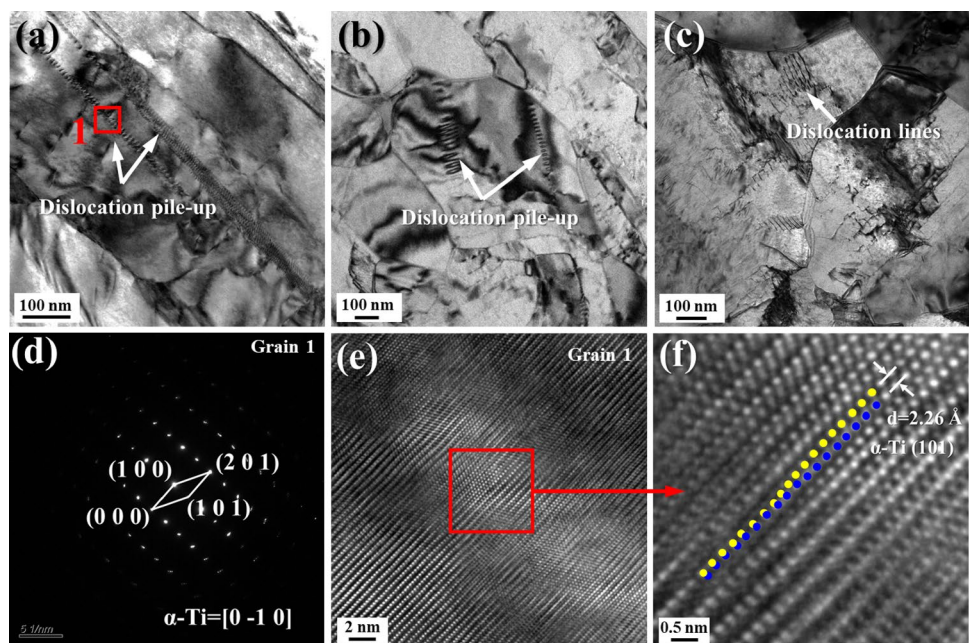


**Fig. 16** Images of the dislocation evolution in the micro-gear center of the formed sample 3# investigated: **a-c** the TEM images of the formed 3# gear center; **d** the diffraction pattern of the grain 1; **e** a HRTEM image of the grain 1 in **a** and **f** the lattice distortion of the box area of **e**

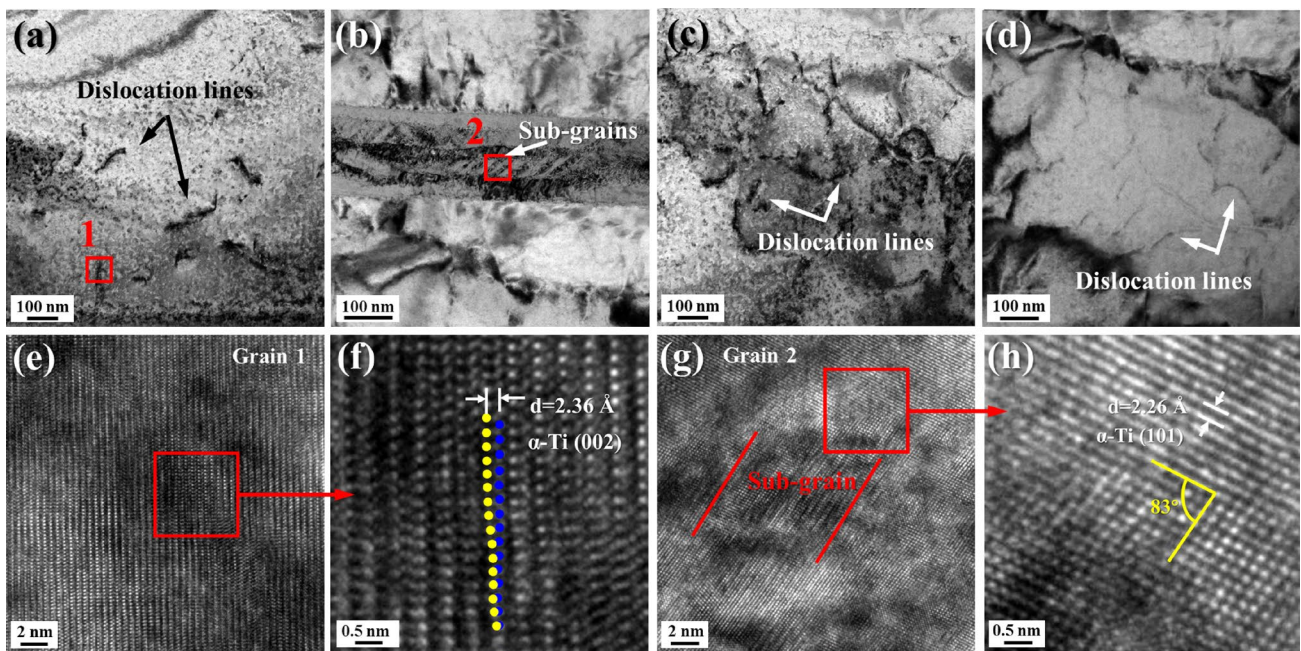
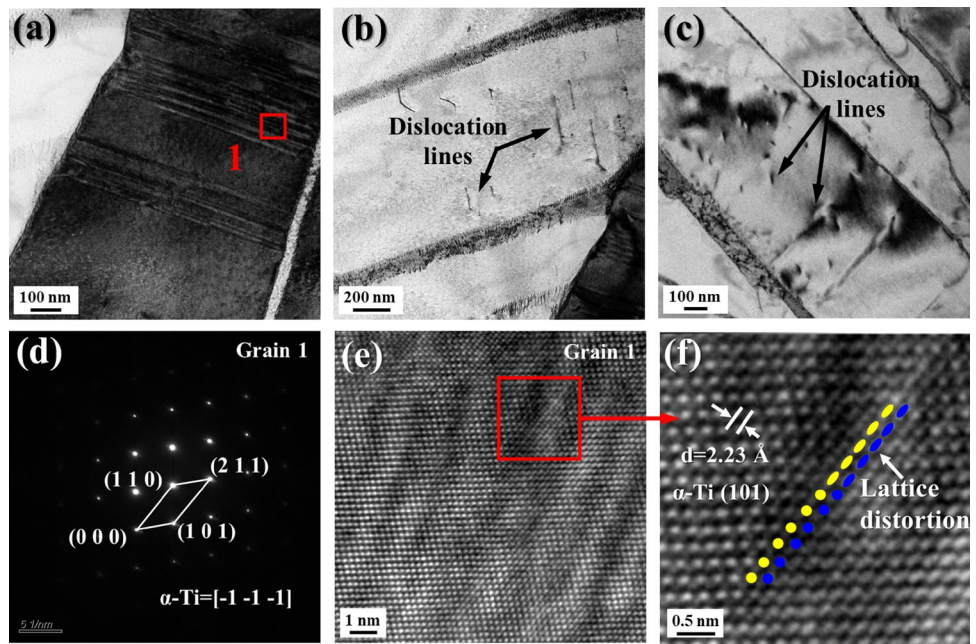


**Fig. 17** Images of the dislocation evolution in the micro-gear tip of the formed sample 3# investigated: **a-d** the TEM images of the formed 3# gear tip; **e** a HRTEM image of the grain 1 in **a**; **f** the lat-

tice distortion of the box area of **e**; **g** a HRTEM image of the grain 2 in **b** and **h** sub-grain angle of the box area of **g**

shows the dislocation in the formed micro-gear center region with the least amount of deformation. As can be seen from Fig. 16a-c, dislocation motion and dislocation density decreased significantly after electric field treatment. The dislocation line becomes shorter and the dislocation pile-up disappears. The reduction of dislocation accumulation is beneficial to the mechanical properties of the material

[52, 53], so the hardness of the gear increases after plastic deformation. Figure 16a shows amount of trans-granular dislocation lines in the  $\alpha$ -Ti grain. More interesting to see is that the atoms are more ordered in the same  $\alpha$ -Ti (101) plane (Fig. 16f) comparing with that in Fig. 15f. This can be explained by the magnetic nail release theory proposed by Molotskii et al. (1995) The dislocation movement will be

easier under the effect of electric field. In motion, the pile-up dislocations spread, and dislocations of burgers vector equal in magnitude and opposite in direction meet to cancel one other out [54], lowering the seen dislocation lines, which is consistent with the EBSD observation.

Furthermore, because of the large deformation, there are some sub-grains formed in the micro-gear tip area (shown in Fig. 17b, g and h). At the same time, the dislocation lines are existed in the gains instead of the dislocation pile-up which is occurred in the raw Ti6Al4V workpiece material specimens. Figure 17f depicts atoms leaving the equilibrium position on the  $\alpha$ -Ti (002) plane, resulting in lattice distortion, which increases atomic potential energy and microscopic stress, and hence increases titanium alloy hardness [55, 56].

In general, on the one hand, the electric field reduces the nucleation activation energy and the growth activation energy of the phase transition, allowing the phase transition of titanium alloy to occur in less time [57]. As a result, the transformation of  $\beta$  to  $\alpha$  phase is accelerated, the phase content is raised, and the hardness of micro-gear is increased. On the other hand, in the process of electric field assisted plastic formation, the electric field accelerates dislocation motion, so that the accumulated dislocation is dispersed and annihilated, and the dislocation lines are reduced. As for the more ordered atomic arrangement of  $\alpha$ -Ti(101) plane and the serious lattice distortion of  $\alpha$ -Ti(002) plane after electric field assisted molding, we will continue to study in the following work.

## 4 Conclusions

In this study, Ti-6Al-4 V micro-gears were successfully prepared in graphite mold by electrically-assisted molding. The whole process has low energy consumption, no sewage discharge and no waste of raw materials. The experimental results show that the total preparation time of the micro-gear is 380s from sample filling (100s), heating and pressurizing (120s), finally cooling (60s) and taking out the sample (100s), and the gear has high precision, good surface quality and higher hardness than the original billet. This study verifies the feasibility of the electro-assisted forming method for the fabrication of titanium alloy micro-gears and provides guidance for the production of other materials and structural micro-components. Specific conclusions are as follows:

(1) When the forming temperature is 1200 °C, the dwell time has a significant impact on the formability of the gear. When the pressure is maintained for 120s, the gear is fully formed with few microstructure defects. Microhardness of the gear is 330.1HV, which is 4.4% improvement over the initial materials.

(2) In titanium alloy billet, the proportion of  $\alpha$  phase is 96.6%, and after forming the gear, the proportion of  $\alpha$  phase is about 99.5%. The increase of  $\alpha$  phase increases the hardness of the gear.

(3) During plastic deformation, phase transformation and recrystallization occurred, which increased the orientation difference of adjacent grains and obtained more large angle grain boundaries.

(4) Under the electro-thermal coupling effect, the gear tip underwent strong plastic deformation in a short time, the grain was refined, the dislocation line lengthened, and the gear tip has the highest peak value of the relative frequency of the average KAM.

(5) The motion of dislocation is easier under the action of electric field. Electron wind plays a major role in dislocation migration, reducing dislocation density and thus improving material plasticity.

**Supplementary Information** The online version contains supplementary material available at <https://doi.org/10.1007/s40684-023-00536-1>.

**Acknowledgements** The authors wish to acknowledge the financial support by the National Nature Science Foundation of China (No.51705348), the Sichuan Science and Technology Program (No. 2021ZHCG0009), and the AVIC Independent Innovation Special Fund Project (No. ZZCX-2021-031). We would like to appreciate the Analytical & Testing Center of Sichuan University for structural characterization work and we would be grateful to Aiqun Gu for her help of EBSD analysis.

**Data Availability** The raw/processed data required to reproduce these findings cannot be shared at this time due to technical or time limitations.

## Declarations

**Conflict of interest** The authors declare that they have no known competing financial interests or personal relationships that could have appeared to influence the work reported in this paper.

**Competing interest** The authors declare that they have no known competing financial interests or personal relationships that could have appeared to influence the work reported in this paper.

## References

- Koç, M., & Mahabunphachai, S. (2007). Feasibility investigations on a novel micro-manufacturing process for fabrication of fuel cell bipolar plates: Internal pressure-assisted embossing of micro-channels with in-die mechanical bonding. *Journal of Power Sources*, 172(2), 725–733. <https://doi.org/10.1016/j.jpowsour.2007.05.089>.
- Azarsa, E., Ibrahim, A., & Papini, M. (2020). Abrasive water and slurry jet micro-machining techniques for fabrication of molds containing raised free-standing micro-features. *Precision Engineering*, 65, 197–215. <https://doi.org/10.1016/j.precisioneng.2020.05.009>.
- Guo, B., Zhang, J., Wu, M., Zhao, Q., Liu, H., Monier, A., & Wang, J. (2020). Water assisted pulsed laser machining of

- micro-structured surface on CVD diamond coating tools. *Journal of Manufacturing Processes*, 56, 591–601. <https://doi.org/10.1016/j.jmapro.2020.04.066>.
4. Davim, J. P. (2023). *Nonconventional Machining*. De Gruyter. <https://doi.org/10.1515/9783110584479>
  5. Davim, J. P. (2013). *Nontraditional Machining Processes*. Springer.
  6. Ali, M. Y., Karim, M., Adesta, A. N., Ismail, E. Y. T., Abdullah, A. F., A. A., & Idris, M. N. (2010). Comparative study of conventional and micro WEDM based on machining of meso/micro Sized Spur Gear. *International Journal of Precision Engineering and Manufacturing*, 11(5), 779–784. <https://doi.org/10.1007/s12541-010-0092-2>.
  7. Wang, Y., Zou, B., & Huang, C. (2019). Tool wear mechanisms and micro-channels quality in micro-machining of Ti-6Al-4V alloy using the Ti(C7N3)-based cermet micro-mills. *Tribology International*, 134, 60–76. <https://doi.org/10.1016/j.triboint.2019.01.030>.
  8. Zhu, J., Lin, Y., Liu, S., Ma, X., & Wang, G. (2020). Plasticity and size effects of micro-forming sheet processed by electropulsing. *Materials and Manufacturing Processes*, 35(10), 1146–1155. <https://doi.org/10.1080/10426914.2020.1772482>.
  9. Davim, J. P. (2013). *Sustainable manufacturing*. John Wiley & Sons.
  10. Yip, W. S., & To, S. (2020). Sustainable Ultra-Precision Machining of Titanium Alloy using intermittent cutting. *International Journal of Precision Engineering and Manufacturing-Green Technology*, 7(2), 361–373. <https://doi.org/10.1007/s40684-019-00078-5>.
  11. Tian, Q., Luo, H., Yi, R., Fan, X., Ma, Y., Shi, D., & Gao, J. (2020). Study of micro-plastic deformation in pure iron before macro-yielding using acoustic emission, electron backscattered diffraction and transmission electron microscopy. *Materials Science and Engineering: A*, 771, 138645. <https://doi.org/10.1016/j.msea.2019.138645>.
  12. Schneider, F., Das, J., Kirsch, B., Linke, B., & Aurich, J. C. (2019). Sustainability in Ultra Precision and Micro Machining: A review. *International Journal of Precision Engineering and Manufacturing-Green Technology*, 6(3), 601–610. <https://doi.org/10.1007/s40684-019-00035-2>.
  13. Qin, Z., Wu, Y., Eizad, A., Lyu, S., & Lee, C. (2021). Advancement of Mechanical Engineering in Extreme environments. *International Journal of Precision Engineering and Manufacturing-Green Technology*, 8(6), 1767–1782. <https://doi.org/10.1007/s40684-020-00295-3>.
  14. Wang, J. L., Fu, M. W., & Shi, S. Q. (2017). Influences of size effect and stress condition on ductile fracture behavior in micro-scaled plastic deformation. *Materials & Design*, 131, 69–80. <https://doi.org/10.1016/j.matdes.2017.06.003>.
  15. Gupta, K., Laubscher, R. F., Davim, J. P., & Jain, N. K. (2016). Recent developments in sustainable manufacturing of gears: A review. *Journal of Cleaner Production*, 112, 3320–3330. <https://doi.org/10.1016/j.jclepro.2015.09.133>.
  16. Chen, X., Wang, Z., Wang, Y., & Chi, G. (2020). Investigation on MRR and machining gap of Micro Reciprocated Wire-EDM for SKD11. *International Journal of Precision Engineering and Manufacturing*, 21(1), 11–22. <https://doi.org/10.1007/s12541-019-00233-7>.
  17. Sun, Q., & Hua, L. (2021). Micro texture of titanium alloys excited nonlinearly by electromagnetic pulse. *Scripta Materialia*, 200, 113.
  18. Xu, M., Li, C., Kurniawan, R., Chen, J., & Ko, T. J. (2022). Influence of different dielectrics and machining parameters for electrical discharge-assisted milling of Titanium Alloy. *International Journal of Precision Engineering and Manufacturing*, 23(10), 1095–1112. <https://doi.org/10.1007/s12541-022-00689-0>.
  19. Faga, M. G., Priarone, P. C., Robiglio, M., Settineri, L., & Tebaldo, V. (2017). Technological and sustainability implications of dry, near-dry, and wet turning of Ti-6Al-4V alloy. *International Journal of Precision Engineering and Manufacturing-Green Technology*, 4(2), 129–139. <https://doi.org/10.1007/s40684-017-0016-z>.
  20. Ortiz, M., Penalva, M., Iriondo, E., & De López, L. N. (2020). Investigation of thermal-related Effects in Hot SPIF of Ti-6Al-4V alloy. *International Journal of Precision Engineering and Manufacturing-Green Technology*, 7(2), 299–317. <https://doi.org/10.1007/s40684-019-00038-z>.
  21. Gupta, M. K., Niesłony, P., Korkmaz, M. E., Kuntoğlu, M., Królczyk, G. M., Günay, M., & Sarıkaya, M. (2023). Comparison of Tool wear, Surface morphology, specific cutting energy and cutting temperature in Machining of Titanium Alloys under Hybrid and Green cooling strategies. *International Journal of Precision Engineering and Manufacturing-Green Technology*. <https://doi.org/10.1007/s40684-023-00512-9>.
  22. Li, W. T., Li, H., & Fu, M. W. (2019). Interactive effect of stress state and grain size on fracture behaviours of copper in micro-scaled plastic deformation. *International Journal of Plasticity*, 114, 126–143. <https://doi.org/10.1016/j.ijplas.2018.10.013>.
  23. Xu, J., Su, Q., Shan, D., & Guo, B. (2019). Sustainable micro-manufacturing of superhydrophobic surface on ultrafine-grained pure aluminum substrate combining micro-embossing and surface modification. *Journal of Cleaner Production*, 232, 705–712. <https://doi.org/10.1016/j.jclepro.2019.05.394>.
  24. Dixit, U. S., Joshi, S. N., & Davim, J. P. (2011). Incorporation of material behavior in modeling of metal forming and machining processes: A review. *Materials & Design*, 32(7), 3655–3670. <https://doi.org/10.1016/j.matdes.2011.03.049>.
  25. Zhou, B., Wang, L., Jin, P., Jia, H., Roven, H. J., Zeng, X., & Li, Y. (2020). Revealing slip-induced extension twinning behaviors dominated by micro deformation in a magnesium alloy. *International Journal of Plasticity*, 128, 102669. <https://doi.org/10.1016/j.ijplas.2020.102669>.
  26. Baral, M., Hama, T., Knudsen, E., & Korkolis, Y. P. (2018). Plastic deformation of commercially-pure titanium: Experiments and modeling. *International Journal of Plasticity*, 105, 164–194. <https://doi.org/10.1016/j.ijplas.2018.02.009>.
  27. Chan, W. L., & Fu, M. W. (2012). Experimental studies of plastic deformation behaviors in microheating process. *Journal of Materials Processing Technology*, 212(7), 1501–1512. <https://doi.org/10.1016/j.jmatprotec.2012.02.013>.
  28. Wang, X., Xu, J., Shan, D., Guo, B., & Cao, J. (2016). Modeling of thermal and mechanical behavior of a magnesium alloy AZ31 during electrically-assisted micro-tension. *International Journal of Plasticity*, 85, 230–257. <https://doi.org/10.1016/j.ijplas.2016.07.008>.
  29. Kou, Z., & Han, F. (2018). On sustainable manufacturing titanium alloy by high-speed EDM milling with moving electric arcs while using water-based dielectric. *Journal of Cleaner Production*, 189, 78–87. <https://doi.org/10.1016/j.jclepro.2018.04.072>.
  30. Cui, W. F., Jin, Z., Guo, A. H., & Zhou, L. (2009). High temperature deformation behavior of  $\alpha + \beta$ -type biomedical titanium alloy Ti-6Al-7Nb. *Materials Science and Engineering: A*, 499(1–2), 252–256. <https://doi.org/10.1016/j.msea.2007.11.109>.
  31. Quan, G., Luo, G., Liang, J., Wu, D., Mao, A., & Liu, Q. (2015). Modelling for the dynamic recrystallization evolution of Ti-6Al-4V alloy in two-phase temperature range and a wide strain rate range. *Computational Materials Science*, 97, 136–147. <https://doi.org/10.1016/j.commatsci.2014.10.009>.
  32. Xia, J., Chai, L., Wu, H., Zhi, Y., Gou, Y., Huang, W., & Guo, N. (2018). EBSD Study of Microstructural and Textural Changes

- of Hot-Rolled Ti–6Al–4V sheet after annealing at 800°C. *Acta Metallurgica Sinica (English Letters)*, 31(11), 1215–1223. <https://doi.org/10.1007/s40195-018-0768-7>.
33. Lee, T., Magargee, J., Ng, M. K., & Cao, J. (2017). Constitutive analysis of electrically-assisted tensile deformation of CP-Ti based on non-uniform thermal expansion, plastic softening and dynamic strain aging. *International Journal of Plasticity*, 94, 44–56. <https://doi.org/10.1016/j.ijplas.2017.02.012>.
  34. Zhao, Z., Wang, G., Zhang, Y., Wang, Y., & Hou, H. (2019). Fast recrystallization and phase transformation in ECAP deformed Ti–6Al–4V alloy induced by pulsed electric current. *Journal of Alloys and Compounds*, 786, 733–741. <https://doi.org/10.1016/j.jallcom.2019.01.328>.
  35. Liu, J., Hassanin, H., Ni, Z., Yang, Y., Yang, G., & Jiang, K. (2017). Production of high-precision micro metallic components by electroforming process. *Materials and Manufacturing Processes*, 32(12), 1325–1330. <https://doi.org/10.1080/10426914.2016.1221092>.
  36. Guo, P., Zhao, Y., Zeng, W., & Hong, Q. (2013). The effect of microstructure on the mechanical properties of TC4-DT titanium alloys. *Materials Science and Engineering: A*, 563, 106–111. <https://doi.org/10.1016/j.msea.2012.11.033>.
  37. Emelianova, E., Romanova, V., Zinovieva, O., & Balokhonov, R. (2020). The effects of surface-layer grain size and texture on deformation-induced surface roughening in polycrystalline titanium hardened by ultrasonic impact treatment. *Materials Science and Engineering: A*, 793, 139896. <https://doi.org/10.1016/j.msea.2020.139896>.
  38. Yan, Z., Wang, D., He, X., Wang, W., Zhang, H., Dong, P., Li, C., Li, Y., Zhou, J., Liu, Z., et al. (2018). Deformation behaviors and cyclic strength assessment of AZ31B magnesium alloy based on steady ratcheting effect. *Materials Science and Engineering: A*, 723, 212–220. <https://doi.org/10.1016/j.msea.2018.03.023>.
  39. Fu, L., He, J., Lu, S., Sun, Y., Zhu, D., & Mao, Y. (2022). Coarsening kinetics of lamellar and equiaxed microstructures of eutectic Au–20Sn during the annealing. *Journal of Materials Research and Technology*, 17, 2134–2144. <https://doi.org/10.1016/j.jmrt.2022.01.162>.
  40. Blum, W., Dvořák, J., Král, P., & Sklenička, V. (2018). Dynamic grain coarsening in creep of pure Cu at 0.42T<sub>m</sub> after predeformation by ECAP. *Materials Science and Engineering: A*, 731, 520–529. <https://doi.org/10.1016/j.msea.2018.05.026>.
  41. Wang, Q., Zhou, R., Guan, J., & Wang, C. (2021). The deformation compatibility and recrystallisation behaviour of the alloy CuSn10P1. *Materials Characterization*, 174, 110940. <https://doi.org/10.1016/j.matchar.2021.110940>.
  42. Liu, Z., Li, P., Xiong, L., Liu, T., & He, L. (2017). High-temperature tensile deformation behavior and microstructure evolution of Ti55 titanium alloy. *Materials Science and Engineering: A*, 680, 259–269. <https://doi.org/10.1016/j.msea.2016.10.095>.
  43. Chen, M., Ma, Y., Lin, Y. C., Lou, Y., Li, H., Wang, G., & Chen, Q. (2022). An innovative annealing treatment method and its mechanism to refine deformed mixed grains of initial aged GH4169 superalloy. *Journal of Alloys and Compounds*, 907, 164325. <https://doi.org/10.1016/j.jallcom.2022.164325>.
  44. Cai, C., Qiu, J. C. D., Shian, T. W., Han, C., Liu, T., Kong, L. B., Srikanth, N., Sun, C., & Zhou, K. (2021). Laser powder bed fusion of Mo2C/Ti-6Al-4V composites with alternately laminated  $\alpha/\beta$  phases for enhanced mechanical properties. *Additive Manufacturing*, 46, 102134. <https://doi.org/10.1016/j.addma.2021.102134>.
  45. Shen, R. R., & Efsing, P. (2018). Overcoming the drawbacks of plastic strain estimation based on KAM. *Ultramicroscopy*, 184, 156–163. <https://doi.org/10.1016/j.ultramicro.2017.08.013>.
  46. Kinsey, B., Cullen, G., Jordan, A., & Mates, S. (2013). Investigation of electroplastic effect at high deformation rates for 304SS and Ti–6Al–4V. *CIRP Annals*, 62(1), 279–282. <https://doi.org/10.1016/j.cirp.2013.03.058>.
  47. Li, D., Yu, E., & Liu, Z. (2013). Microscopic mechanism and numerical calculation of electroplastic effect on metal's flow stress. *Materials Science and Engineering: A*, 580, 410–413. <https://doi.org/10.1016/j.msea.2013.05.052>.
  48. Xiang, S., & Zhang, X. (2019). Dislocation structure evolution under electroplastic effect. *Materials Science and Engineering: A*, 761, 138026. <https://doi.org/10.1016/j.msea.2019.138026>.
  49. Biesuz, M., Saunders, T., Ke, D., Reece, M. J., Hu, C., & Grasso, S. (2021). A review of electromagnetic processing of materials (EPM): Heating, sintering, joining and forming. *Journal of Materials Science & Technology*, 69, 239–272. <https://doi.org/10.1016/j.jmst.2020.06.049>.
  50. Zhang, H., & Zhang, X. (2020). Uniform texture in Al-Zn-Mg alloys using a coupled force field of electron wind and external load. *Journal of Materials Science & Technology*, 36, 149–159. <https://doi.org/10.1016/j.jmst.2019.07.025>.
  51. Chen, K., Zhan, L., Xu, Y., & Liu, Y. (2020). Effect of pulsed current density on creep-aging behavior and microstructure of AA7150 aluminum alloy. *Journal of Materials Research and Technology*, 9(6), 15433–15441. <https://doi.org/10.1016/j.jmrt.2020.10.100>.
  52. Liu, C., Xie, L., Qian, D., Hua, L., Wang, L., & Zhang, L. (2021). Microstructure evolution and mechanical property response of TC11 titanium alloy under electroshock treatment. *Materials & Design*, 198, 109322. <https://doi.org/10.1016/j.matdes.2020.109322>.
  53. Davim, J. P. (2015). *Materials forming and machining: Research and Development*. Elsevier.
  54. Ma, R., & Zhang, X. (2022). Improvement of mechanical properties and microstructural refining of cast titanium alloys by coupling of electropulsing and temporary alloying element hydrogen. *Materials Science and Engineering: A*, 858, 144176. <https://doi.org/10.1016/j.msea.2022.144176>.
  55. Guo, H., Liu, P., Qin, X., Song, Y., Qian, D., Xie, L., Wang, L., Zhang, L., & Hua, L. (2021). Electroshock treatment dependent microstructural evolution and mechanical properties of near- $\beta$  titanium alloy manufactured by directed energy deposition. *Materials & Design*, 212, 110286. <https://doi.org/10.1016/j.matdes.2021.110286>.
  56. Yan, X., Zhang, S., Huang, K., Yang, Y., Wang, W., & Wu, M. (2022). Effect of Holding Time on the Extrusion Force and Microstructure Evolution during the Plastic Forming of Ti-6Al-4V Micro-Gears. *Materials*, 15(4), 1507. <https://doi.org/10.3390/ma15041507>.
  57. Xiao, A., Yan, Z., Huang, C., Yu, Z., Wang, S. & Cui, X. (2023). Reduction of springback of Ti-6Al-4V alloy by high-density and instantaneous pulsed current. *Materials Science and Engineering: A*, 877, 145188. <https://doi.org/10.1016/j.msea.2023.145188>

**Publisher's Note** Springer Nature remains neutral with regard to jurisdictional claims in published maps and institutional affiliations.

Springer Nature or its licensor (e.g. a society or other partner) holds exclusive rights to this article under a publishing agreement with the author(s) or other rightsholder(s); author self-archiving of the accepted manuscript version of this article is solely governed by the terms of such publishing agreement and applicable law.



**Bo Zeng** is a PhD student at School of Mechanical Engineering Sichuan University, Chengdu, Sichuan, China. His research interests include electric field assisted forming.



**Jie Wang** is the Dean of the School of Mechanical Engineering Sichuan University. He obtained his Ph. D. degree in 2000, and his research direction is electric field assisted manufacturing.



**Xiangzhong Yan** is a PhD student at School of Mechanical Engineering Sichuan University, Chengdu, Sichuan, China. His research interests include plastic forming and Micro component manufacturing.



**Kunlan Huang** is an associate professor at the School of Mechanical Engineering Sichuan University. She received her PhD in 2015. Her research interest is special energy field assisted manufacturing technology.



**Zhiqiang Xie** is Chief Technologist of AECC AERO Science and Technology Co., Ltd, Doctor of materials science and Engineering, graduated from Chongqing University in 2020. His research direction is advanced material processing technology.



**Yi Yang** is the doctoral supervisor of Material Processing in the School of Mechanical Engineering Sichuan University, and a visiting scholar in the University of Strathclyde, UK. His research direction is micromanufacturing and special molding process methods.



**Jian Liu** is the doctoral supervisor of Material Processing Major in the School of Mechanical Engineering Sichuan University. He received his PhD degree in 2014 from the University of Birmingham, UK, and his research direction is advanced manufacturing.